# Strong coupling of Sm and Fe magnetism in SmFeAsO as revealed by magnetic x-ray scattering

S. Nandi,[1,*] Y. Su,[2] Y. Xiao,[1] S. Price,[1] X. F. Wang,[3] X. H. Chen,[3] J. Herrero-Martín,[4] C. Mazzoli,[4] H. C. Walker,[4] L. Paolasini,[4] S. Francoual,[5] D. K. Shukla,[5] J. Strempfer,[5] T. Chatterji,[6] C. M. N. Kumar,[1] R. Mittal,[7] H. M. Rønnow,[8] Ch. Rüegg,[9,10] D. F. McMorrow,[10] and Th. Brückel[1,2]

[1]*Jülich Centre for Neutron Science JCNS and Peter Grünberg Institut PGI, JARA-FIT, Forschungszentrum Jülich GmbH, D-52425 Jülich, Germany*

[2]*Jülich Centre for Neutron Science JCNS-FRM II, Forschungszentrum Jülich GmbH, Outstation at FRM II, Lichtenbergstraße 1, D-85747 Garching, Germany*

[3]*Hefei National Laboratory for Physical Science at Microscale and Department of Physics, University of Science and Technology of China, Hefei, Anhui 230026, People's Republic of China*

[4]*European Synchrotron Radiation Facility, BP 220, F-38043 Grenoble Cedex 9, France*

[5]*Deutsches Elektronen-Synchrotron DESY, D-22607 Hamburg, Germany*

[6]*Institut Laue-Langevin, BP 156, F-38042 Grenoble Cedex 9, France*

[7]*Solid State Physics Division, Bhabha Atomic Research Centre, Trombay, Mumbai 400 085, India*

[8]*Laboratory for Quantum Magnetism, Ecole Polytechnique Fédérale de Lausanne (EPFL), CH-1015 Lausanne, Switzerland*

[9]*Laboratory for Neutron Scattering, Paul Scherrer Institut, CH-5232 Villigen PSI, Switzerland*

[10]*London Centre for Nanotechnology and Department of Physics and Astronomy, University College London, London WC1E 6BT, United Kingdom*

(Received 3 July 2011; published 5 August 2011)

The magnetic structures adopted by the Fe and Sm sublattices in SmFeAsO have been investigated using element-specific x-ray resonant and nonresonant magnetic scattering techniques. Between 110 and 5 K, the Sm and Fe moments are aligned along the $c$ and $a$ directions, respectively, according to the same magnetic representation $\Gamma_5$ and the same propagation vector $(1\ 0\ \frac{1}{2})$. Below 5 K, the magnetic order of both sublattices changes to a different magnetic structure, and the Sm moments reorder in a magnetic unit cell equal to the chemical unit cell. Modeling of the temperature dependence for the Sm sublattice, as well as a change in the magnetic structure below 5 K, provides clear evidence of a surprisingly strong coupling between the two sublattices, and indicates the need to include anisotropic exchange interactions in models of SmFeAsO and related compounds.

DOI: 10.1103/PhysRevB.84.054419 PACS number(s): 74.70.Xa, 75.25.−j, 75.50.Ee

## I. INTRODUCTION

Following the discovery of superconductivity in $LaFeAsO_{1-x}F_x$, with $T_c = 26$ K,[1] an increase of the superconducting transition temperature to above 50 K has been achieved by replacing La with rare-earth ($R$) elements.[2–6] The highest transition temperature is observed in $SmFeAsO_{1-x}F_x$ ($T_c \sim 55$ K). Interestingly, several studies on powder samples indicate that Sm magnetic order coexists with superconductivity over a range of fluorine doping.[7–9] Muon-spin relaxation measurements on $R$FeAsO ($R$ = La, Ce, Pr, and Sm) compounds found considerable interaction between the rare-earth and Fe magnetism below the ordering of Fe moments ($T \sim 140$ K) only in CeFeAsO.[10] This leads to the conclusion that the $R$-Fe interaction may not be crucial for the observed enhanced superconductivity in $R$FeAsO$_{1-x}$F$_x$. Recent neutron-scattering measurements on NdFeAsO also found an interaction between the two magnetic sublattices, however at $T \sim 15$ K, much below the ordering temperature of the Fe moments.[11] In the case of $EuFe_2As_2$,[12,13] the only known rare-earth containing member of the $AFe_2As_2$ ($A$ = alkaline earth, rare earth) family, no interaction has been found so far. Therefore, elucidating the interaction between the two sublattices and determining its nature is an important endeavor in understanding magnetism and superconductivity in the $R$FeAsO family.

Due to the strong neutron absorption of Sm, the magnetic structure determination in SmFeAsO via neutron diffraction is considerably more challenging than that of other members of the new superconductors. The only attempt was made on a powder sample.[14] Here we report on the first element-specific x-ray resonant magnetic scattering (XRMS) and nonresonant x-ray magnetic scattering (NRXMS) studies of SmFeAsO to explore the details of the magnetic structure of the parent compound and to determine the interaction between the two magnetic sublattices. Our resonant scattering experiments show that there is a strong interplay between Fe and Sm magnetism. Magnetic order of Sm exists at temperatures as high as 110 K and can be explained by the coupling between Sm and Fe magnetism.

## II. EXPERIMENTAL DETAILS

Single crystals of SmFeAsO were grown using NaAs flux as described earlier.[15] For the scattering measurements, an as-grown platelike single crystal of approximate dimensions $2 \times 2 \times 0.1$ mm$^3$ with a surface perpendicular to the $c$ axis was selected. The XRMS and NRXMS experiments were performed on the ID20 beamline[16] at the ESRF (European Synchrotron Radiation Facility) in Grenoble, France at the Sm $L_2$, $L_3$ and Fe $K$ absorption edges and at the Fe $K$ edge at beamline P09 at the PETRA III synchrotron at DESY. The incident radiation was linearly polarized parallel to the horizontal scattering plane ($\pi$ polarization) and perpendicular to the vertical scattering plane ($\sigma$ polarization) for the ID20 and P09 beamlines, respectively. The spatial cross section of the beam was 0.5 (horizontal) × 0.5 (vertical) mm$^2$ for the ID20 while it was 0.2 (horizontal) × 0.1 (vertical) mm$^2$ for P09.

 

Au (2 2 0) was used at the Sm $L_2$ edge, and Cu (2 2 0) was used for both the Sm $L_3$ and Fe $K$ absorption edges as a polarization and energy analyzer to suppress the charge and fluorescence background relative to the magnetic scattering signal. The sample was mounted at the end of the cold finger of a standard orange cryostat (at ID20), a vertical field cryomagnet (at ID20) and a displex refrigerator (at P09) with the $ac$ plane coincident with the scattering plane. Measurements at ID20 were performed at temperatures between 1.6 K and 15 K, while the lowest achievable temperature at P09 was 5 K.

## III. EXPERIMENTAL RESULTS

### A. Macroscopic characterizations

Figure 1 shows the heat capacity of a SmFeAsO single crystal, measured using a Quantum Design physical property measurement system (PPMS). Specific-heat data show phase transitions at $143.5 \pm 2$ K and $4.8 \pm 0.2$ K, respectively. Figure 2(a) shows the magnetic susceptibility of a SmFeAsO single crystal, measured using a Quantum Design (SQUID) magnetometer. Magnetic susceptibility shows a clear phase transition at 5 K. There is a clear anomaly $\chi_{ab} > \chi_c$ over the whole temperature range. Figure 2(b) shows the $M$-$H$ curves at several temperatures for magnetic fields parallel to both the $c$ and $ab$ planes, measured using a Quantum Design vibrating sample magnetometer (VSM). Zero-field intercept of the $M$-$H$ curves for both field directions places an upper limit of ferromagnetic contribution less than $1.7 \times 10^{-6}$ $\mu_B$/f.u. for all the temperatures measured.

### B. Observation of resonant and nonresonant magnetic scattering and characterization of the transition temperatures

To determine whether there is a structural phase transition, as observed in powder SmFeAsO,[17] $(\xi\ \xi\ 0)_T$ scans were performed through the tetragonal $(T)$ $(2\ 2\ 6)_T$ Bragg reflection as a function of temperature. As shown in the inset of Fig. 3(a), the $(2\ 2\ 6)_T$ Bragg reflection splits into orthorhombic $(O)$ $(4\ 0\ 6)_O$ and $(0\ 4\ 6)_O$ Bragg reflections below $T_S = 140 \pm 1$ K. This splitting is consistent with the structural phase transition from space group $P4/nmm$ to $Cmme$. The orthorhombic distortion $\delta$[17,18] increases with decreasing temperature without any noticeable change at the 5 K phase transition. We note that the transition temperature $T_S$ is consistent with the peak observed in specific-heat data. In the remainder of the paper, we will use orthorhombic crystallographic notation.

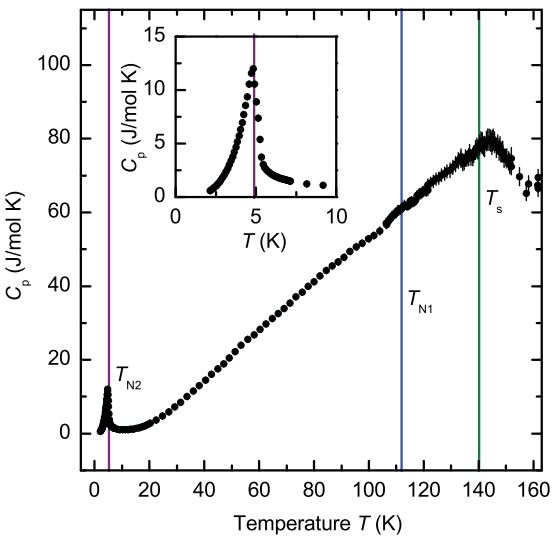


FIG. 1. (Color online) Temperature dependence of the specific heat. $T_{N1}$ and $T_{N2}$ are the spontaneous magnetic ordering temperatures of the Fe and Sm magnetic moments respectively. $T_S$ is the structural phase transition temperature. Vertical lines are guides to the eye after x-ray diffraction measurements.

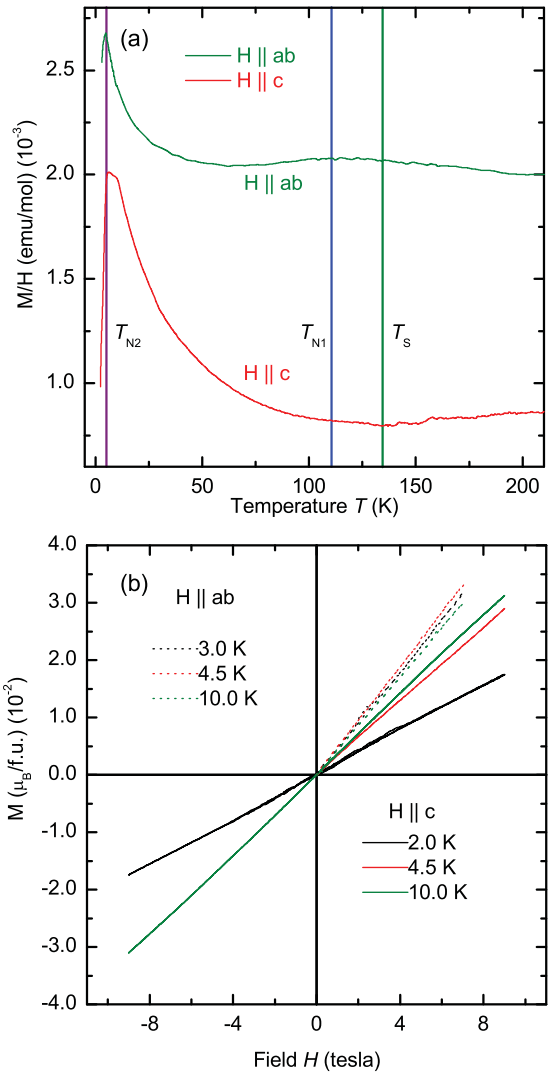


FIG. 2. (Color online) (a) Temperature dependence of the magnetic susceptibility measured upon heating of the zero-field cooled sample in a field of 1 T. (b) $M$-$H$ curves for magnetic fields parallel and perpendicular to the $c$ direction at several temperatures.

Below $T_{N1} = 110$ K, a magnetic signal was observed at the reciprocal lattice points characterized by the propagation vector $(1\ 0\ \frac{1}{2})$ when the x-ray energy was tuned through the Sm $L_2$ and Fe $K$ edges, indicating the onset of Sm and Fe magnetic order, respectively. Figure 3(b) shows a very similar temperature evolution of the nonresonant and the resonant signal at the Fe $K$ edge for the (1 0 6.5) reflection, supporting

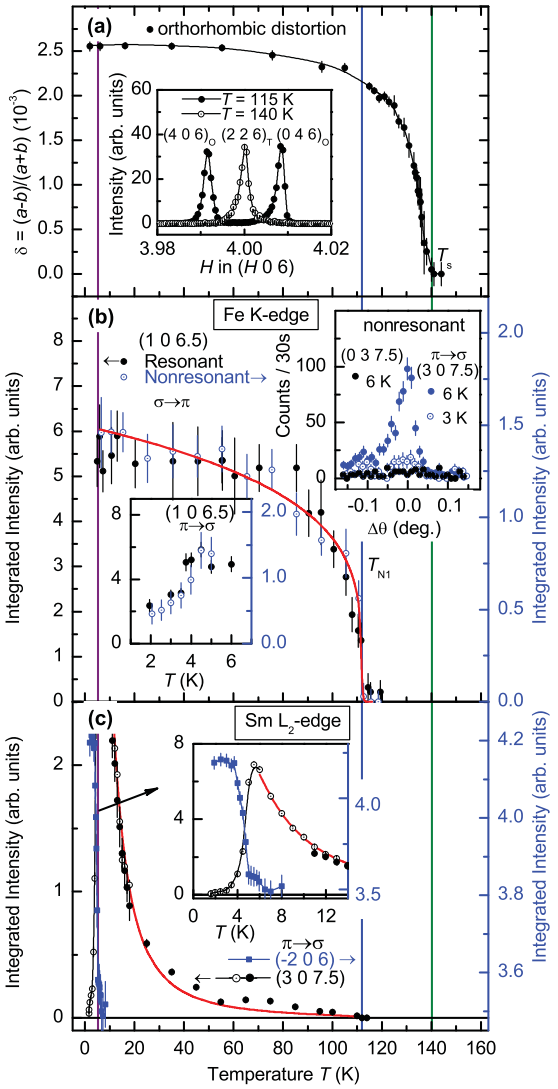


FIG. 3. (Color online) (a) Temperature dependence of the orthorhombic distortion. Inset shows ($\xi$ 0 0) scans through the (4 0 6) reflection. (b) Temperature dependence of the (1 0 6.5) reflection measured in both resonant (at $E = 7.106$ keV, which is 6 eV below the Fe $K$-edge energy of 7.112 keV) and nonresonant (100 eV below the Fe $K$ edge) conditions at P09 with a displex. Lower inset shows temperature dependence of the (1 0 6.5) reflection measured using the cryomagnet. All other measurements below 5 K were performed using the orange cryostat. Upper inset shows rocking scans at the (3 0 7.5) and (0 3 7.5) reflections at selected temperatures. (c) Temperature dependencies of the (3 0 7.5) and (−2 0 6) reflections measured in resonant condition ($E = 7.314$ keV) at the Sm $L_2$ edge. Open (closed) circles represent measurements with (without) attenuation of the primary beam. Solid thin lines serve as guides to the eye while thick lines (red) show fit as described in the text.

the magnetic origin of the resonant signal. The resonant signal was measured at the maximum in the resonant scattering ($E = 7.106$ keV) at the Fe $K$ edge, while the nonresonant signal was measured approximately 100 eV below the Fe $K$ edge. Temperature dependence of this reflection below 5 K (lower inset) together with rocking scans shown in the upper inset confirm that the iron magnetic order changes below 5 K. Figure 3(c) depicts the temperature evolution of the (3 0 7.5) and (−2 0 6) reflections measured at the Sm $L_2$ edge at resonance ($E = 7.314$ keV). At $T_{N2} = 5$ K, the intensity of the (3 0 7.5) reflection drops quickly to zero, and reappears at the position of the charge (−2 0 6) reflection, signaling a change in the magnetic order of Sm with the magnetic unit cell equal to the chemical unit cell. Here we note that all the measurements below 15 K require significant attenuation (transmission ∼10% of the incident beam) of the beam to reduce sample heating.

To confirm the resonant magnetic behavior of the peaks, we performed energy scans at the Sm $L_2$, $L_3$, and Fe $K$ absorption edges as shown in Fig. 4.[19,20] At 6 K, at the Sm $L_2$ edge, we observed a dipole resonance peak ∼2 eV above the absorption edge for both the (1 0 7.5) and (−2 0 6) reflections. We note that for the (−2 0 6) reflection, charge and magnetic peak coincide. Therefore, measurement of a magnetic signal which is five to six orders of magnitude weaker than the Thomson charge scattering requires significant reduction of the charge background. The charge background can be reduced significantly by a factor of $\cos^2 2\theta_{\text{analyzer}} \times \cos^2 2\theta_{\text{sample}}$ in the $\pi \rightarrow \sigma$ geometry for reflections with a scattering angle ($2\theta_{\text{sample}}$) close to 90°.[21] The (−2 0 6) reflection with scattering angles ($2\theta_{\text{sample}}$) of ∼86° and ∼95° at the Sm $L_2$ and Sm $L_3$ edges, respectively, fulfills these conditions. The charge signal is reduced by a factor of $\sim 7 \times 10^{-6}$ with the scattering angle of the analyzer ($2\theta_{\text{analyzer}}$) close to 92° for both the edges. Thus, measurement of magnetic signal seems feasible for the (−2 0 6) reflection in the $\pi \rightarrow \sigma$ geometry. Figure 4(b) shows energy scans through the (−2 0 6) reflection at 2 K and 6 K. Subtraction of the energy scan at 6 K from 2 K shows a pronounced resonance feature at the same energy as that observed for the charge-forbidden (1 0 7.5) reflection. Similar energy scans were performed at the Sm $L_3$ edge and are shown in Figs. 4(d) and 4(e). In addition to the dipole feature observed at the $L_2$ edge, a quadrupole feature appears approximately 6 eV below the Sm $L_3$ edge. We note that the change in the energy spectra from the Sm $L_2$ to the $L_3$ edge is consistent with the observed resonance in another intermetallic compound containing Sm.[22]

Figure 4(c) shows the energy scan through the Fe $K$ edge. Several features are observable in the energy spectrum: (a) Resonant features at and above $E = 7.106$ keV and (b) an energy independent nonresonant signal for energies below the resonant features. The nonresonant signal is about a factor of 2.5 smaller than the resonant signal. The overall energy spectrum is similar to that observed in previous XRMS measurements in the $\sigma \rightarrow \pi$ scattering channel at the transition metal $K$ edges for the $BaFe_2As_2$,[23] $Ce(Co_{0.07}Fe_{0.97})_2$,[20] and NiO[24] compounds. It is noteworthy that the pre-edge sharp resonant feature observed at $E = 7.106$ keV for SmFeAsO is also present in all of the above-mentioned compounds. It appears at an energy corresponding to the pre-edge hump observed in the respective absorption (fluorescence) spectrum. The broad resonant feature above $E = 7.106$ keV is also present in all the above compounds, however, its relative intensity compared to the sharp feature varies from one compound to another.

Further confirmation that the dipole and quadrupole resonances at the $L_2$ and $L_3$ edges are magnetic is obtained from the same temperature dependence of the dipole and quadrupole

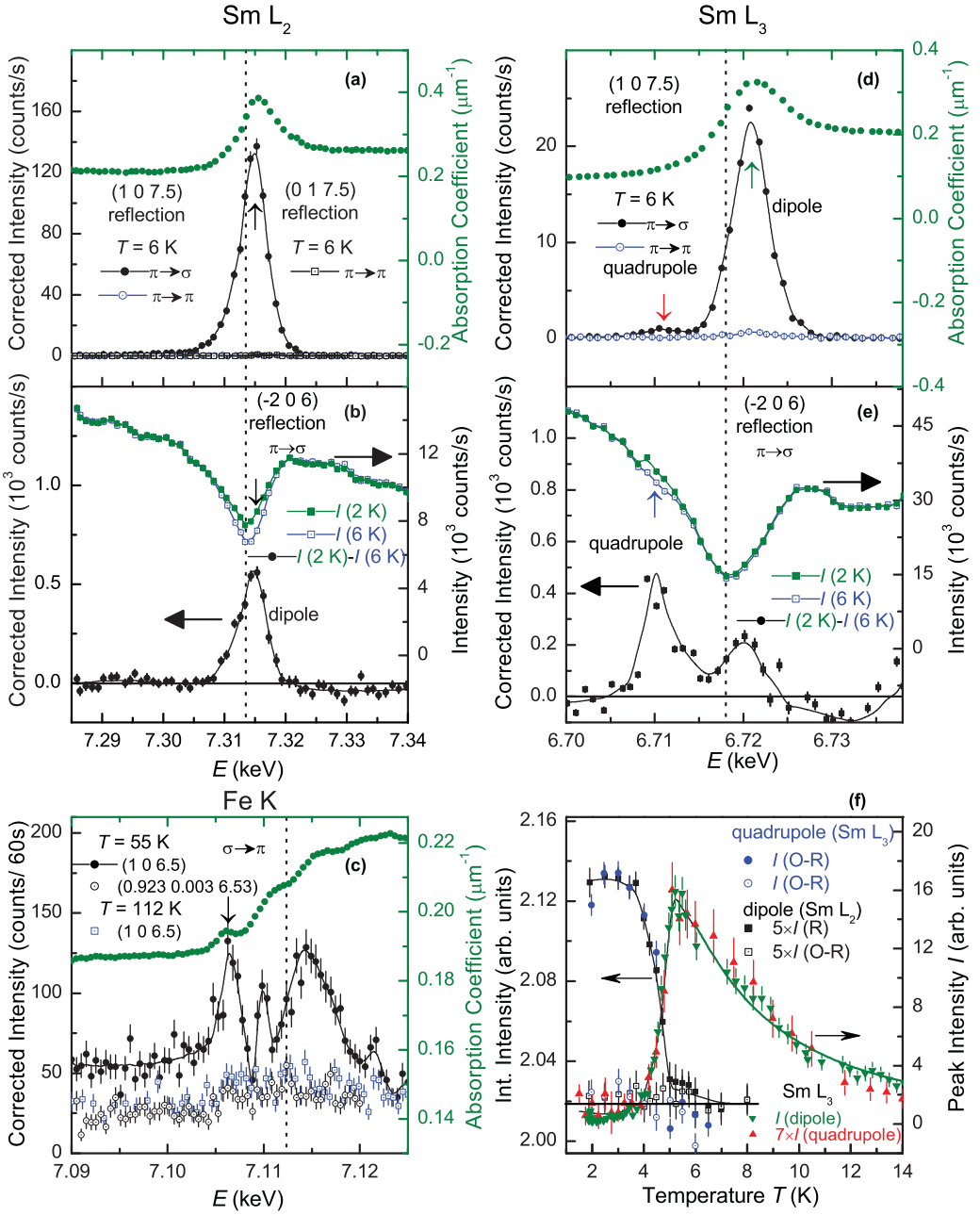


FIG. 4. (Color online) (a), (b), (d), (e) Energy scans of the (1 0 7.5), (0 1 7.5), and (−2 0 6) reflections and of the absorption coefficient at the Sm $L_2$ (left panel) and $L_3$ edges (right panel). The dashed lines depict the Sm $L_2$ and $L_3$ absorption edges as determined from the inflection point of the absorption coefficient. The absorption coefficient was calculated and the intensity was corrected following the recipe described in Refs. 19 and 20. (c) Energy scans of the absorption coefficient and of the (1 0 6.5) reflection below ($T = 55$ K, filled circles) and above ($T = 112$ K, open squares) $T_{N1}$, and the measured background at $T = 55$ K away from the magnetic Bragg peak (open circles). The dashed line depicts the Fe $K$ edge. (f) Comparison of the temperature dependences of the dipole and quadrupole resonances for the (−2 0 6) and (1 0 7.5) reflections, respectively. For the (−2 0 6) reflection, integrated intensity was measured approximately 30 eV below (off-resonance, O-R) the observed resonance (R, $E = 6.710$ keV and 7.314 keV for the Sm $L_3$ and $L_2$ edges, respectively) to show the temperature dependence of the pure charge signal. The intensities have not been corrected for absorption. In (a)–(e), vertical arrows indicate the energies at which temperature dependences of the resonant signal were measured for Figs. 3(b) and 3(c) and Fig. 4(f). In (a)–(f), lines serve as guides to the eye.

resonances as shown in Fig. 4(f) for both the (−2 0 6) and (1 0 7.5) reflections. Since the quadrupole signal is directly related to the ordering of the 4$f$ moments, the similarity of the temperature dependences of both resonances implies that both the dipole and quadrupole resonances are purely magnetic.

### C. Magnetic structure in the temperature range 5 K ⩽ $T$ ⩽ 110 K

We now turn to the determination of the magnetic moment configuration for the Sm moments in the temperature range $T_{N2} \leqslant T \leqslant T_{N1}$. For the crystallographic space group $Cmme$,

TABLE I. Basis vectors for the space group *Cmme* with $\mathbf{k}_{17} = (0,1,0.5)$. The decomposition of the magnetic representation for the Sm site (0,0.25,0.137) is $\Gamma_{\text{Mag}} = 1\Gamma_1^1 + 1\Gamma_2^1 + 0\Gamma_3^1 + 1\Gamma_4^1 + 1\Gamma_5^1 + 0\Gamma_6^1 + 1\Gamma_7^1 + 1\Gamma_8^1$. The atoms of the nonprimitive basis are defined according to 1 (0,0.25,0.137), 2 (0,0.75,0.863). Lattice parameters of the orthorhombic crystal at 100 K[17]: $a = 5.5732$ Å, $b = 5.5611$ Å, $c = 8.4714$ Å.

| | | | | | Magnetic intensity | | | |
|---|---|---|---|---|---|---|---|---|
| | | BV components | | | $(h\ 0\ \frac{l}{2})$ | | $(0\ k\ \frac{l}{2})$ | |
| IR | Atom | $m_{\|a}$ | $m_{\|b}$ | $m_{\|c}$ | $\pi \to \sigma$ | $\pi \to \pi$ | $\pi \to \sigma$ | $\pi \to \pi$ |
| $\Gamma_1$ | 1 | 1 | 0 | 0 | Yes | No | No | Yes |
| | 2 | −1 | 0 | 0 | | | | |
| $\Gamma_2$ | 1 | 0 | 1 | 0 | No | Yes | Yes | No |
| | 2 | 0 | 1 | 0 | | | | |
| $\Gamma_4$ | 1 | 0 | 0 | 1 | Yes | No | Yes | No |
| | 2 | 0 | 0 | 1 | | | | |
| $\Gamma_5$ | 1 | 0 | 0 | 1 | Yes | No | Yes | No |
| | 2 | 0 | 0 | −1 | | | | |
| $\Gamma_7$ | 1 | 0 | 1 | 0 | No | Yes | Yes | No |
| | 2 | 0 | −1 | 0 | | | | |
| $\Gamma_8$ | 1 | 1 | 0 | 0 | Yes | No | No | Yes |
| | 2 | 1 | 0 | 0 | | | | |

and a propagation vector of the form $(1\ 0\ \frac{1}{2})$, six independent magnetic representations (MRs) are possible.[25] All the MRs along with the calculated intensities for different polarization geometries are listed in Table I. Among all the MRs, $\Gamma_8$ (F) and $\Gamma_1$ (AF) MRs allow magnetic moment along $a$, $\Gamma_2$ (F) and $\Gamma_7$ (AF) along $b$, and $\Gamma_4$ (F) and $\Gamma_5$ (AF) along the $c$ direction, respectively. Here, F and AF denote ferro and antiferromagnetic alignment between Sm(1) and Sm(2) moments, respectively [see Fig. 5(b)]. For a second-order phase transition, Landau theory predicts that only one of the six above-mentioned MRs is realized at the phase transition.[25] We note that the $\pi \to \pi$ scattering geometry is sensitive only to the moment perpendicular to the scattering plane for the dipole resonance.[26] Since no magnetic signal was observed at the (0 1 7.5) (sensitive to $\Gamma_1$ and $\Gamma_8$) and (1 0 7.5) (sensitive to $\Gamma_2$ and $\Gamma_7$) reflections in the $\pi \to \pi$ scattering channel at the Sm $L_2$ edge [see Figs. 4(a)–4(d)], we can exclude the moment in the $a$ and $b$ directions and hence, the MRs $\Gamma_1$, $\Gamma_8$, $\Gamma_2$, and $\Gamma_7$. To differentiate between the MRs $\Gamma_4$ and $\Gamma_5$ (the moment along the $c$ direction), the integrated intensities for a series of $(1\ 0\ \frac{l}{2})$ reflections were measured [see Fig. 5(a)] and compared with the calculated intensity as outlined below. The intensity for a particular reflection can be written as

$$I = SAL|F_m|^2, \tag{1}$$

where $S$ is the arbitrary scaling factor, $A = \frac{\sin(\theta+\alpha)}{\sin\theta\cos\alpha}$ is the absorption correction, and $L = \frac{1}{\sin 2\theta}$ is the Lorentz factor. Here, $\alpha$ is the angle that the scattering vector $\mathbf{Q}$ $(= \mathbf{k_f} - \mathbf{k_i})$ makes with the crystallographic $c$ direction perpendicular to the surface of the sample, and $\theta$ is half of the scattering angle. $\alpha$ is positive (negative) for larger (smaller) angles for the outgoing beam with respect to the sample surface. $|F_m|$ is the modulus of the magnetic structure factor. The magnetic

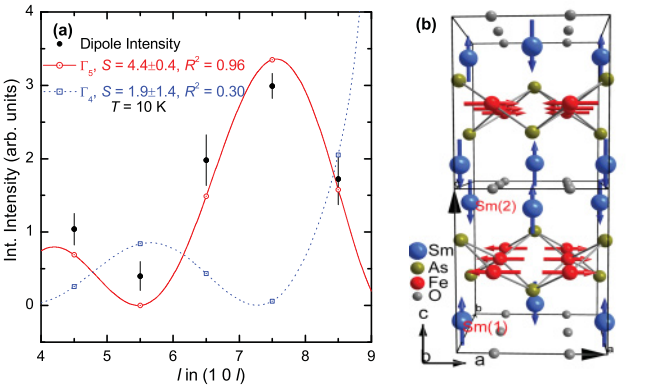


FIG. 5. (Color online) (a) $l$ dependence of the integrated intensity at the Sm $L_2$ edge along with the fits for the $(1\ 0\ \frac{l}{2})$ reflections. Open symbols are the calculated intensities. Lines serve as guides to the eye. (b) Proposed magnetic structure in the temperature range $5\ \text{K} \leqslant T \leqslant 110\ \text{K}$.

structure factor $F_m$ for the $(h\ k\ l)$ reflections can be written as

$$F_m = \sum_j f_j e^{2\pi i(hx_j + ky_j + lz_j)}. \tag{2}$$

The summation is over all the magnetic atoms in the unit cell. $f_j$ is the resonant (nonresonant) magnetic scattering amplitude which is listed for different polarization geometries by Hill and McMorrow for XRMS[26] and by Blume and Gibbs for NRXMS.[27] In particular, $f_j$ depends on the polarization geometry as well as the moment direction. $x_j$,$y_j$ and $z_j$ are the atomic position of the $j$th atom within the unit cell. The angular dependence of the magnetic structure factor originates from the magnetic scattering amplitude $f_j$. For dipole resonance and for the $\pi \to \sigma$ geometry, $f_j \propto \mathbf{k_i} \cdot \boldsymbol{\mu}$,[26,28] where $\mathbf{k_i}$ and $\boldsymbol{\mu}$ are the wave vectors of the incoming photons and the magnetic moment, respectively. For the dipole resonance, and for the reflections of the type $(1\ 0\ \frac{l}{2})$, $|F_m|^2$ is proportional to $\sin^2(2\pi zl)\sin^2(\theta+\alpha)$ and $\cos^2(2\pi zl)\sin^2(\theta+\alpha)$ for the $\Gamma_4$ and $\Gamma_5$ MRs, respectively. $z = 0.137$ is the atomic position of Sm moments within the unit cell.[17] While the $\sin^2(2\pi zl)/\cos^2(2\pi zl)$ term comes from the relative orientation of the magnetic moment within the magnetic unit cell, the term $\sin^2(\theta+\alpha)$ comes from the dot product between $\mathbf{k_i}$ and $\boldsymbol{\mu}$ [$(90^\circ - \theta - \alpha)$ is the angle between $\mathbf{k_i}$ and $\boldsymbol{\mu}$]. We note that there is only one free parameter for the dipole intensity [see Eq. (1)], namely the arbitrary scaling factor $S$. Figure 5(a) shows a fit to the observed intensities for the two above-mentioned MRs. Since the model calculation with the magnetic moment in the $\Gamma_5$ MR closely agrees with the observed intensity, we conclude that the magnetic Sm moments are arranged according to the MR $\Gamma_5$.

For the determination of the MR for the Fe moments, the nonresonant signal was measured at 15 K. Similar representation analysis provides six possible MRs for the magnetic order of Fe. All the MRs along with the calculated intensities for different polarization geometries are listed in Table II. Among all the MRs, $\Gamma_5$ and $\Gamma_6$ MRs allow magnetic moment along $a$, $\Gamma_3$ and $\Gamma_4$ along $b$, and $\Gamma_1$ and $\Gamma_2$ along the $c$ direction, respectively. Among the two MRs for a particular moment direction, the first one represents F alignment of the

TABLE II. Basis vectors for the space group *Cmme* with $\mathbf{k}_{17} = (0,1,0.5)$. The decomposition of the magnetic representation for the Fe site (0.75,0,0.5) is $\Gamma_{\text{Mag}} = 1\Gamma_1^1 + 1\Gamma_2^1 + 1\Gamma_3^1 + 1\Gamma_4^1 + 1\Gamma_5^1 + 1\Gamma_6^1 + 0\Gamma_7^1 + 0\Gamma_8^1$. The atoms of the nonprimitive basis are defined according to 1 (0.75,0,0.5), 2 (0.75,0.5,0.5).

| | | | | | Magnetic intensity | | | |
|---|---|---|---|---|---|---|---|---|
| | | BV components | | | $(h\,0\,\frac{l}{2})$ | | $(0\,k\,\frac{l}{2})$ | |
| IR | Atom | $m_{\parallel a}$ | $m_{\parallel b}$ | $m_{\parallel c}$ | $\pi \to \sigma$ | $\pi \to \pi$ | $\pi \to \sigma$ | $\pi \to \pi$ |
| $\Gamma_1$ | 1 | 0 | 0 | 1 | Yes | No | No | No |
| | 2 | 0 | 0 | 1 | | | | |
| $\Gamma_2$ | 1 | 0 | 0 | 1 | No | No | Yes | No |
| | 2 | 0 | 0 | −1 | | | | |
| $\Gamma_3$ | 1 | 0 | 1 | 0 | No | Yes | No | No |
| | 2 | 0 | 1 | 0 | | | | |
| $\Gamma_4$ | 1 | 0 | 1 | 0 | No | No | Yes | No |
| | 2 | 0 | −1 | 0 | | | | |
| $\Gamma_5$ | 1 | 1 | 0 | 0 | Yes | No | No | No |
| | 2 | 1 | 0 | 0 | | | | |
| $\Gamma_6$ | 1 | 1 | 0 | 0 | No | No | No | Yes |
| | 2 | −1 | 0 | 0 | | | | |

magnetic moments along $b$ and AF alignment along $a$, while the second one represents exactly the opposite alignment in the respective directions. $\Gamma_2$, $\Gamma_3$, $\Gamma_4$, and $\Gamma_6$ MRs can be excluded from the fact that finite intensity was observed for the (1 0 6.5) reflection in the $\pi \to \sigma$ geometry (see Table II). Zero intensities for the (0 3 7.5) reflection in the $\pi \to \sigma$ geometry [see inset of Fig. 3(b)] and of the (1 0 6.5) reflection in the $\pi \to \pi$ channel are also consistent with the absence of $\Gamma_4$ and $\Gamma_3$ MRs, respectively. Finite intensity of the (1 0 6.5) reflection in the $\pi \to \sigma$ channel implies that the moments are within the $a$–$c$ scattering plane, i.e., $\Gamma_1$ and $\Gamma_5$ are the possible MRs. We measured the off-specular reflections (3 0 7.5) and $(\bar{3}\,0\,7.5)$ to determine the moment direction. The angular dependence of the nonresonant magnetic scattering cross section for the $\pi \to \sigma$ geometry, $f_j = -2\sin^2\theta \mathbf{k_f} \cdot \boldsymbol{S}$ (assuming a spin-only magnetic moment of iron),[27] is different for these two reflections providing strong sensitivity to the moment direction. $\mathbf{k_f}$ and $\boldsymbol{S}$ are the wave vectors of the outgoing photons and the spin magnetic moment, respectively. The ratio can be written as

$$\frac{I\left(h0\frac{l}{2}\right)}{I\left(\bar{h}\,0\frac{l}{2}\right)} = \frac{\sin(\theta-\alpha)\cos^2(\theta-\alpha)}{\sin(\theta+\alpha)\cos^2(\theta+\alpha)}. \tag{3}$$

The calculated ratio $I(3\,0\,7.5)/I(\bar{3}\,0\,7.5)$ amounts to 5.2 and 0.35 for moments along the $a$ and $c$ directions, respectively. The experimentally determined ratio $6.5 \pm 0.9$ confirms that the moments are in the $a$ direction, i.e., the MR is $\Gamma_5$. We note that this is the same MR as that of Sm, which is expected if there is significant coupling between the two magnetic sublattices. Arrangements of the magnetic moments according to the MR $\Gamma_5$ is shown in Fig. 5(b).

### D. Temperature dependence of the magnetic intensity in the temperature range 5 K $\leqslant T \leqslant$ 110.0 K

Although the ordering temperatures are the same for both the Fe and Sm sublattices, the order parameters are qualitatively different, as can be seen from Figs. 3(b) and 3(c). Particularly, the order parameter for the Sm moment is quite unusual. Very similar temperature dependence of the Ce sublattice magnetization in CeFeAsO has been obtained indirectly using muon-spin relaxation measurements.[10] With reference to other systems, this unusual behavior can be explained with a ground-state doublet crystal-field level, split by an exchange field.[29,30] The Kramer's $Sm^{3+}$ions in SmFeAsO are at the positions of local point symmetry $C_{2v}$ and, therefore, must have a doublet ground state. At low temperatures, only the ground-state doublet is appreciably populated, because the energy difference between the ground-state and the next crystal electric-field levels, in general, is large and of the order of 17 meV in the case of CeFeAsO.[31] Taking into account only the ground-state doublet and a splitting $\triangle(T)$, we can write

$$m_z^{\text{Sm}}(T) = \frac{g_j \mu_B}{2} \tanh\left[\frac{\Delta(T)}{2k_B T}\right], \tag{4}$$

where $\Delta(T) = g_J \mu_B B_z^{\text{eff}}(T)$ is the splitting of the ground-state doublet by the effective field produced by the Fe sublattice. $g_J = \frac{2}{7}$ is the Landé $g$ factor of the free $Sm^{3+}$, and $\mu_B$ is the Bohr magneton. The effective field should be proportional to the ordered magnetic moment of Fe, and can be written as

$$B_z^{\text{eff}}(T) = B_0\left(1 - \frac{T}{T_N}\right)^{\beta}. \tag{5}$$

Since the observed intensity is proportional to the square of the ordered magnetic moment ($I = \text{A m}^2$), $T_N$ ($= 110 \pm 1$ K) and $\beta$ ($= 0.112 \pm 0.008$) can be extracted from a fit to the integrated intensity for the (1 0 6.5) reflection in Fig. 3(b). A fit to the temperature dependence of the (3 0 7.5) reflection in Fig. 3(c) over the whole temperature range gives $B_0 = (56.4 \pm 1.9)$ T and the corresponding $\triangle(T = 0) = (0.93 \pm 0.03)$ meV. We note that the value of $B_0$ characterizing the strength of interaction between the two sublattices is comparable or even higher than the value for Ce-Fe interaction in CeFeAsO.[10,32] The value of $\triangle = 0.93$ meV is comparable to the ground-state splitting of Ce crystal electric field levels of 0.9 meV in CeFeAsO, measured using inelastic neutron scattering.[31]

### E. Magnetic structure below $T \leqslant$ 5.0 K

For the low-temperature phase ($T \leqslant 5.0$ K), the determination of the magnetic structure of the Sm subsystem is considerably more difficult due to the overlap of the magnetic intensity with the charge intensity. Magnetization measurements with magnetic fields along the $c$ direction and in the $ab$ plane exclude ferromagnetic arrangement in the respective direction (plane) [see Fig. 2(b)]. There remain three antiferromagnetic representations along the $a$, $b$, and c directions. The relative change in magnetization below 5 K is much more pronounced for a magnetic field applied along the $c$ direction than in the $ab$ plane [see Fig. 2(a)]. Therefore, we conclude that the Sm moments are aligned along the $c$ direction below 5 K, which is in agreement with recent neutron-scattering measurements.[14]

To determine the magnetic structure of the Fe moments below $T = 5$ K, a number of possible propagation vectors

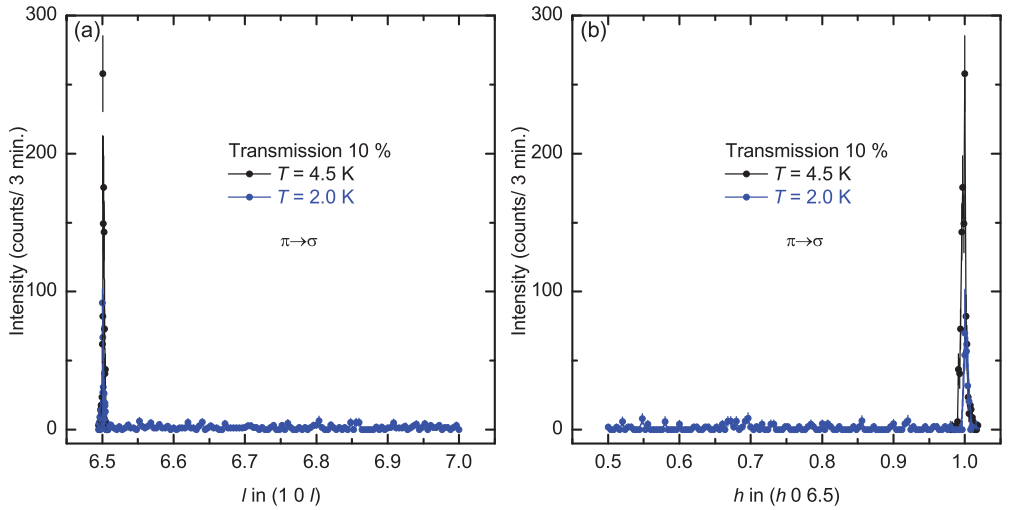


FIG. 6. (Color online) (a) and (b) $l$ and $h$ scans through the (1 0 6.5) reflection. 10% of the incident beam was used to reduce the sample heating. For comparison, scans at $T = 4.5$ K is plotted together with scans taken at $T = 2.0$ K. We noticed that the sample heating is much greater in the cryomagnet than in the orange cryostat. The remaining intensity at $T = 2$ K is due to the residual sample heating in the cryomagnet.

suggested for the *R*FeAsO family,[10] (1 0 0.5), (1 0 0), (0.5 0 0.5), and (0 0 0.5), were checked by rocking scans with a counting time (∼3 min/data point) a factor of three larger than other measurements at 2 K. Measurements were performed in both the $\pi \rightarrow \sigma$ and $\pi \rightarrow \pi$ channels to exclude possible reorientation of the magnetic moments from the $a$ to $b$ direction. Additionally, long scans along the $h$ and $l$ directions for the (1 0 6.5) reflections were performed to exclude possible incommensurate order in the respective directions (see Fig. 6). However, no signal was observed for the above measurements. The magnetic structure with the same propagation vector as that of Sm implies a Néel-type in-plane structure, which is impossible to check with hard x rays given the weakness of the resonant (nonresonant) signal and the overlap of the magnetic signal with the charge signal. In NdFeAsO, a change in the coupling along the $c$ axis (AFM to FM) has been observed upon the spontaneous order of Nd.[11] However, this is not the case here, as confirmed by the absence of the scattering signal at the (1 0 7) reflection as shown in Fig. 7. The absence of the scattering signal in the positions mentioned above indicates that the in-plane as well as out-of plane correlations are modified upon the spontaneous ordering of Sm. This observation is unique among the *R*FeAsO family and indicates an intricate interplay between the two sublattices. Here we note that the rare-earth sites project onto the centers of the Fe plaquettes, and thus isotropic interactions between the two vanish by symmetry. Hence, anisotropic exchange interactions play a major role in determining the spin structure of the Fe sublattice and should be studied theoretically to understand the magnetism in the *R*FeAsO family.

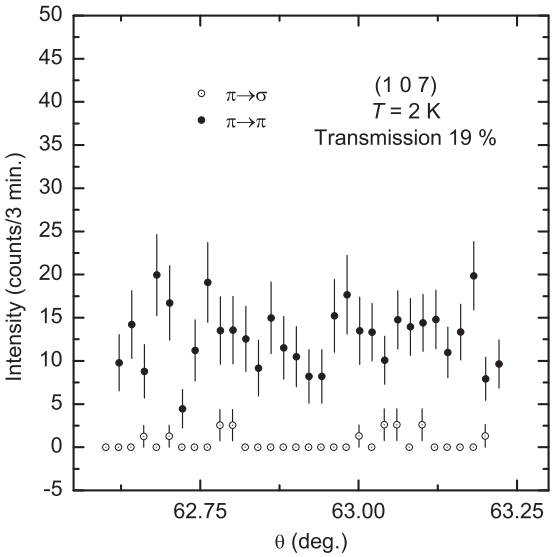


FIG. 7. (Color online) Rocking scans through the (1 0 7) reflection in both the $\pi \rightarrow \sigma$ and $\pi \rightarrow \pi$ channels. Higher background in the $\pi \rightarrow \pi$ channel is mainly due to the less suppression of the fluorescence background.

## IV. CONCLUSION

In summary, using XRMS and NRXMS we found that between 110 K and 5 K, the Sm moments are aligned in the $c$ direction while Fe moments are aligned in the $a$ direction according to the same MR $\Gamma_5$ and the propagation vector $(1\ 0\ \frac{1}{2})$. Modeling of the temperature dependence indicates that the Sm moments are induced by the exchange field of the Fe moments. Below 5 K, the magnetic order of both sublattices changes to a different magnetic structure, indicating an intricate interplay between the two magnetic sublattices. Our finding of an intricate interplay between the magnetism of Sm and Fe in the SmFeAsO compound sheds light on the currently debated importance of the $R$-Fe interaction in the family of iron-based superconductors.

## ACKNOWLEDGMENTS

S.N. would like to acknowledge S. Adiga, M. Angst, B. Schmitz, T. Trenit, and S. Das for technical help.

*s.nandi@fz-juelich.de


[1] Y. Kamihara, T. Watanabe, M. Hirano, and H. Hosono, J. Am. Chem. Soc. **130**, 3296 (2008).

[2] X. H. Chen, T. Wu, G. Wu, R. H. Liu, H. Chen, and D. F. Fang, Nature (London) **453**, 761 (2008).

[3] C. Wang, L. Li, S. Chi, Z. Zhu, Z. Ren, Y. Li, Y. Wang, X. Lin, Y. Luo, and S. Jiang, Europhys. Lett. **83**, 67006 (2008).

[4] Z.-A. Ren, J. Yang, W. Lu, W. Yi, X.-L. Shen, Z.-C. Li, G.-C. Che, X.-L. Dong, L.-L. Sun, and F. Zhou, Europhys. Lett. **82**, 57002 (2008).

[5] H. Kito, H. Eisaki, and A. Iyo, J. Phys. Soc. Jpn. **77**, 063707 (2008).

[6] J.-W. G. Bos, G. B. S. Penny, J. A. Rodgers, D. A. Sokolov, A. D. Huxley, and J. P. Attfield, Chem. Commun. **31**, 3634 (2008).

[7] M. Tropeano, A. Martinelli, A. Palenzona, E. Bellingeri, E. Galleani d'Agliano, T. D. Nguyen, M. Affronte, and M. Putti, Phys. Rev. B **78**, 094518 (2008).

[8] L. Ding, C. He, J. K. Dong, T. Wu, R. H. Liu, X. H. Chen, and S. Y. Li, Phys. Rev. B **77**, 180510 (2008).

[9] A. J. Drew, C. Niedermayer, P. J. Baker, F. L. Pratt, S. J. Blundell, T. Lancaster, R. H. Liu, G. Wu, X. H. Chen, I. Watanabe, V. K. Malik, A. Dubroka, M. Rössle, K. W. Kim, C. Baines, and C. Bernhard, Nat. Mater. **8**, 310 (2009).

[10] H. Maeter, H. Luetkens, Y. G. Pashkevich, A. Kwadrin, R. Khasanov, A. Amato, A. A. Gusev, K. V. Lamonova, D. A. Chervinskii, R. Klingeler, C. Hess, G. Behr, B. Böchner, and H.-H. Klauss, Phys. Rev. B **80**, 094524 (2009).

[11] W. Tian, W. Tian, W. Ratcliff, M. G. Kim, J.-Q. Yan, P. A. Kienzle, Q. Huang, B. Jensen, K. W. Dennis, R. W. McCallum, T. A. Lograsso, R. J. McQueeney, A. I. Goldman, J. W. Lynn, and A. Kreyssig, Phys. Rev. B **82**, 060514 (2010).

[12] J. Herrero-Martín, V. Scagnoli, C. Mazzoli, Y. Su, R. Mittal, Y. Xiao, T. Brueckel, N. Kumar, S. K. Dhar, A. Thamizhavel, Luigi Paolasini, Phys. Rev. B **80**, 134411 (2009).

[13] Y. Xiao, Y. Su, M. Meven, R. Mittal, C. M. N. Kumar, T. Chatterji, S. Price, J. Persson, N. Kumar, S. K. Dhar, A. Thamizhave, and Th. Brueckel, Phys. Rev. B **80**, 174424 (2009).

[14] D. H. Ryan, J. M. Cadogan, C. Ritter, F. Canepa, A. Palenzona, and M. Putti, Phys. Rev. B **80**, 220503 (2009).

[15] J.-Q. Yan, S. Nandi, J. L. Zarestky, W. Tian, A. Kreyssig, B. Jensen, A. Kracher, K. W. Dennis, R. J. McQueeney, A. I. Goldman, R. W. McCallum, and T. A. Lograsso, Appl. Phys. Lett. **95**, 222504 (2009).

[16] L. Paolasini, C. Detlefs, C. Mazzoli, S. Wilkins, P. P. Deen, A. Bombardi, N. Kernavanois, F. de Bergevin, F. Yakhou, J. P. Valade, I. Breslavetz, A. Fondacaro, G. Pepellin, and P. Bernard, J. Synchrotron Radiat. **14**, 301 (2007).

[17] A. Martinelli, A. Palenzona, C. Ferdeghini, M. Putti, and H. Emerich, J. Alloys Compd. **477**, L21 (2009).

[18] S. Nandi, M. G. Kim, A. Kreyssig, R. M. Fernandes, D. K. Pratt, A. Thaler, N. Ni, S. L. Bud'ko, P. C. Canfield, J. Schmalian, R. J. McQueeney, and A. I. Goldman, Phys. Rev. Lett. **104**, 057006 (2010).

[19] M. K. Sanyal, D. Gibbs, J. Bohr, and M. Wulff, Phys. Rev. B **49**, 1079 (1994).

[20] L. Paolasini, S. Di Matteo, P. P. Deen, S. Wilkins, C. Mazzoli, B. Detlefs, G. Lapertot, and P. Canfield, Phys. Rev. B **77**, 094433 (2008).

[21] J. W. Kim, A. Kreyssig, P. Ryan, E. Mun, P. C. Canfield, and A. I. Goldman, Appl. Phys. Lett. **90**, 202501 (2007).

[22] C. Adriano, R. Lora-Serrano, C. Giles, F. de Bergevin, J. C. Lang, G. Srajer, C. Mazzoli, L. Paolasini, and P. G. Pagliuso, Phys. Rev. B **76**, 104515 (2007).

[23] M. G. Kim, A. Kreyssig, Y. B. Lee, J. W. Kim, D. K. Pratt, A. Thaler, S. L. Bud'ko, P. C. Canfield, B. N. Harmon, R. J. McQueeney, and A. I. Goldman, Phys. Rev. B **82**, 180412 (2010).

[24] W. Neubeck, C. Vettier, F. deBergevin, F. Yakhou, D. Mannix, O. Bengone, M. Alouani, and A. Barbier, Phys. Rev. B **63**, 134430 (2001).

[25] A. S. Wills, Physica B **276–278**, 680 (2000).

[26] J. P. Hill and D. F. McMorrow, Acta Crystallogr. Sect. A **52**, 236 (1996).

[27] M. Blume and D. Gibbs, Phys. Rev. B **37**, 1779 (1988).

[28] T. Brückel, D. Hupfeld, J. Strempfer, W. Caliebe, K. Mattenberger, A. Stunault, N. Bernhoeft, and G. J. McIntyre, Eur. Phys. J. B **19**, 475 (2001).

[29] R. Sachidanandam, T. Yildirim, A. B. Harris, A. Aharony, and O. Entin-Wohlman, Phys. Rev. B **56**, 260 (1997).

[30] S. Nandi, A. Kreyssig, L. Tan, J. W. Kim, J. Q. Yan, J. C. Lang, D. Haskel, R. J. McQueeney, and A. I. Goldman, Phys. Rev. Lett. **100**, 217201 (2008).

[31] S. Chi, D. T. Adroja, T. Guidi, R. Bewley, S. Li, J. Zhao, J. W. Lynn, C. M. Brown, Y. Qiu, G. F. Chen, J. L. Lou, N. L. Wang, and P. Dai, Phys. Rev. Lett. **101**, 217002 (2008).

[32] A. Jesche, C. Krellner, M. de Souza, M. Lang, and C. Geibel, New J. Phys. **11**, 103050 (2009).